



DIGITAL ACCESS TO SCHOLARSHIP AT HARVARD

Affinity flow fractionation of cells via transient interactions with asymmetric molecular patterns

The Harvard community has made this article openly available.
[Please share](#) how this access benefits you. Your story matters.

| | |
|--------------------------|------------------------------------------------------------------------------------------------------------------------------------------------------------------------------------------------------------------------------------------------------------------------------------------------------------------------------------------------------------------------------------------------------|
| Citation | Bose, Suman, Rishi Singh, Mikhail Hanewich-Hollatz, Chong Shen, Chia-Hua Lee, David M. Dorfman, Jeffrey M. Karp, and Rohit Karnik. 2013. "Affinity flow fractionation of cells via transient interactions with asymmetric molecular patterns." <i>Scientific Reports</i> 3 (1): 2329. doi:10.1038/srep02329. http://dx.doi.org/10.1038/srep02329 . |
| Published Version | doi:10.1038/srep02329 |
| Accessed | April 17, 2018 4:34:35 PM EDT |
| Citable Link | http://nrs.harvard.edu/urn-3:HUL.InstRepos:11717635 |
| Terms of Use | This article was downloaded from Harvard University's DASH repository, and is made available under the terms and conditions applicable to Other Posted Material, as set forth at http://nrs.harvard.edu/urn-3:HUL.InstRepos:dash.current.terms-of-use#LAA |

(Article begins on next page)



OPEN

Affinity flow fractionation of cells via transient interactions with asymmetric molecular patterns

SUBJECT AREAS:

LABORATORY
TECHNIQUES AND
PROCEDURES

LAB-ON-A-CHIP

BIOMATERIALS-CELLS

BIOMEDICAL ENGINEERING

Suman Bose¹, Rishi Singh¹, Mikhail Hanewich-Hollatz¹, Chong Shen¹, Chia-Hua Lee², David M. Dorfman³, Jeffrey M. Karp^{4,5} & Rohit Karnik¹

¹Department of Mechanical Engineering, Massachusetts Institute of Technology, MA 02139, USA, ²Department of Materials Science and Engineering, Massachusetts Institute of Technology, MA 02139, USA, ³Department of Pathology, Brigham & Women's Hospital, Harvard Medical School, Boston, MA 02115, USA, ⁴Harvard-MIT Division of Health Sciences and Technology, Massachusetts Institute of Technology, MA 02139, USA, ⁵Division of Biomedical Engineering, Department of Medicine, Center for Regenerative Therapeutics, Brigham and Women's Hospital, Harvard Medical School, Boston, MA 02115, USA.

Received
24 May 2013Accepted
10 July 2013Published
31 July 2013

Correspondence and requests for materials should be addressed to J.M.K. (jeffkarp@mit.edu) or R.K. (karnik@mit.edu)

Flow fractionation of cells using physical fields to achieve lateral displacement finds wide applications, but its extension to surface molecule-specific separation requires labeling. Here we demonstrate affinity flow fractionation (AFF) where weak, short-range interactions with asymmetric molecular patterns laterally displace cells in a continuous, label-free process. We show that AFF can directly draw neutrophils out of a continuously flowing stream of blood with an unprecedented 400,000-fold depletion of red blood cells, with the sorted cells being highly viable, unactivated, and functionally intact. The lack of background erythrocytes enabled the use of AFF for direct enumeration of neutrophils by a downstream detector, which could distinguish the activation state of neutrophils in blood. The compatibility of AFF with capillary microfluidics and its ability to directly separate cells with high purity and minimal sample preparation will facilitate the design of simple and portable devices for point-of-care diagnostics and quick, cost-effective laboratory analysis.

Isolation of cells from complex mixtures such as blood and bone marrow is of immense importance in disease diagnosis^{1,2}, stem cell therapeutics³, genetic analysis⁴, and other applications. Microfluidic technologies for label-free separation of cells offer the advantages of simpler operation, lower cost, and faster time-to-result, and are emerging as important tools for point-of-care diagnostics⁵. Many of these technologies belong to a class of separations known as flow fractionations, wherein cells flowing in a microchannel are displaced perpendicular to the direction of flow under the action of a force, which results in continuous sorting. Currently, flow fractionation of cells is limited to long-range physical forces arising from dielectrophoresis, acoustophoresis, gravitational, magnetic, or inertial effects. The non-specific action of these long-range force fields limits the use of flow fractionation of cells to a few applications, while its extension to sorting based on molecular recognition requires pre-labeling of cells with magnetic or dielectric beads⁶. In contrast, transient interactions of molecules on the cell with adhesive molecules patterned asymmetrically on a surface can exert forces on the cell to deflect it perpendicular to the direction of fluid flow, without capture^{7–10}. This effect requires weak-affinity molecular interactions to avoid irreversible cell capture and provides a new paradigm for label-free flow fractionation of cells, called affinity flow fractionation (AFF).

Nature has evolved a number of molecules that exhibit weak, yet relatively specific adhesive interactions including bacterial adhesion molecules¹¹, selectins involved in homing of circulating cells¹², and MHC-II molecules on antigen presenting cells that exhibit weak affinity towards the T-cell receptor¹³. Among them, P-selectin is a model protein whose kinetics of interaction with its ligand are well characterized. P-selectin exhibits specificity for neutrophils over other leukocytes and is involved in recruitment of neutrophils during the early phase of inflammation¹⁴. A simple device for isolation of neutrophils from blood would be useful in a number of diagnostic applications including detection of sepsis¹⁵, discrimination between bacterial and viral infection¹⁶, and for HLA typing².

Here we report affinity flow fractionation (AFF) of neutrophils from human blood using surfaces decorated with asymmetric patterns of P-selectin. The significance of the current method is that it is the first demonstration of flow fractionation of cells directly from blood purely based on molecular interactions, allowing very high

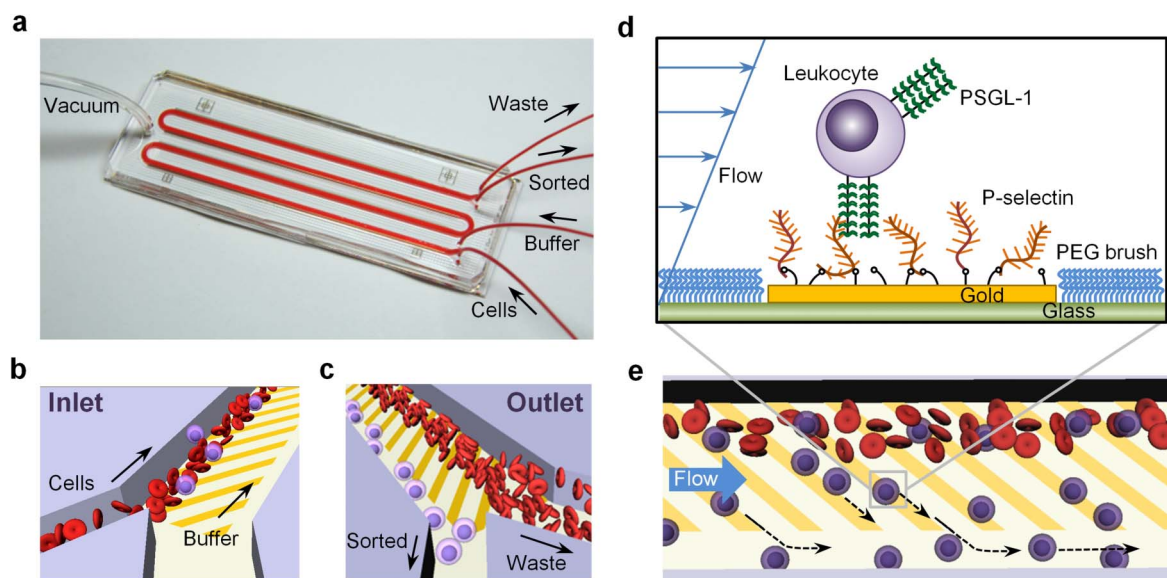


Figure 1 | Design of the microfluidic cell separation device. The device consists of a serpentine channel with two inlet and outlet ports (a). The cell mixture is injected parallel to a buffer stream into the device (b) and a pure stream of target cells is retrieved from the outlet port (c). The straight segments of the microfluidic separation channel are patterned with parallel gold stripes grafted with P-selectin (d), which allows the target cells to interact with the patterns and roll on them (e). The asymmetry of the patterns with respect to the flow alters the trajectories of the target cells such that they roll along the edge of the pattern (shown with dotted line) and get displaced into the buffer stream.

rejection of non-interacting cells (> 5 log depletion of RBCs). The sorted leukocytes were highly enriched for viable, non-activated, and intact neutrophils with greater than 92% purity. Using a cell line that interacts with P-selectin to study the distribution of cells undergoing AFF, we developed a mathematical transport model that accounts for the key phenomena and accurately predicts the separation process. Finally, exploiting the activation-induced changes in interaction of neutrophils with P-selectin, we demonstrate the potential of using the current technology for developing quick point-of-care tests for detecting sepsis and other inflammatory conditions.

Results

The AFF device accepts a sample stream of blood or a mixture of cells and a buffer stream, which then run parallel in a 20 cm-long separation channel (Fig. 1, Supplementary Fig. S1). The cells settle under the influence of gravity along the length of the separation channel, allowing them to interact with inclined molecular patterns at the bottom of the channel. For sorting of neutrophils, we use P-selectin patterns comprising parallel strips (15 μm in width) aligned at 15° to the direction of fluid flow to maximize their lateral displacement¹⁷. The desired pattern was replicated in gold on a glass slide using photolithography. The gold region was activated using 3,3'-dithiopropionic acid di(N-succinimidyl ester) while the glass was passivated using PEG-silane, following which the substrate was incubated with P-selectin solution which led to immobilization of the P-selectin molecules specifically to the gold region. Target cells that interact with the P-selectin patterns are displaced laterally into the buffer stream and eventually reach the non-patterned gutter region that allows for quick elution of the separated cells. The novel surface functionalization created a robust antifouling surface that resulted in minimal non-specific adhesion of cells and platelets in both normal and activated blood. The bends in the serpentine channel do not have P-selectin patterns (Supplementary Fig. S1) and are free from curvature effects due to the low Reynolds and Dean numbers (~ 0.1 and ~ 0.01 , respectively). Thus the bends do not contribute to dispersion of cells during the separation process.

Length-dependent, PSGL-1 specific sorting of model cell lines. To investigate the transport of cells in the device, we studied the

separation of HL60 cells from K562 cells, both of which are myeloid in origin. HL60 cells express PSGL-1 (the major ligand for P-selectin)¹⁸ and exhibit 'cell rolling' on P-selectin surfaces, which is a process involving continuous formation and breakage of bonds between the cell and the surface under the influence of hydrodynamic shear¹⁸. K562 cells do not exhibit strong interactions with P-selectin surfaces¹⁹. A mixture of fluorescently stained HL60 and K562 cells was injected into the device alongside a buffer stream (Supplementary Fig. S2) at a wall shear stress of 0.5 dyn/cm², which enabled effective cell capture and separation as discussed later. Over the 20 cm length of the separation channel, the mean position of HL60 cells was displaced laterally by ~ 800 μm , and about 80% of the HL60 cells were found to be concentrated in a narrow band on the sorted side (Fig. 2a). The separation process is visualized using the distribution of the cell flux at different downstream locations, represented as a probability density that indicates the relative resolution of separation between the two cell types as they flow along the separation channel (Fig. 2b). This probability density can be used to calculate the purity (percentage of target cells in sorted sample) and recovery (percentage of total target cells sorted) of the HL60 cells at a particular downstream location, depending on the fraction of the total flow collected as the sorted stream (Fig. 2c). As a higher fraction of flow is collected as the sorted stream, the recovery increases, while the purity monotonically decreases. Tuning the fraction of the flow collected as the sorted stream determines the trade-off between purity and recovery, depending on the needs of the application. For example, collecting 25% of the flow in the sorted stream yielded a purity of 94.6% and recovery of 83% as measured by flow cytometry (Supplementary Fig. S3).

Control experiments were used to verify that the cell separation was due to P-selectin/PSGL-1 interactions. HL60 cells were not laterally displaced when BSA was immobilized on the gold patterns instead of P-selectin (Fig. 2b), or when PSGL-1 on the cells was blocked with an antibody (Supplementary Fig. S4a). Furthermore, in the absence of P-selectin, there was no significant difference between distribution of cells on the BSA passivated substrates with or without the gold patterns (Fig. 2b and Supplementary Fig. S4b),

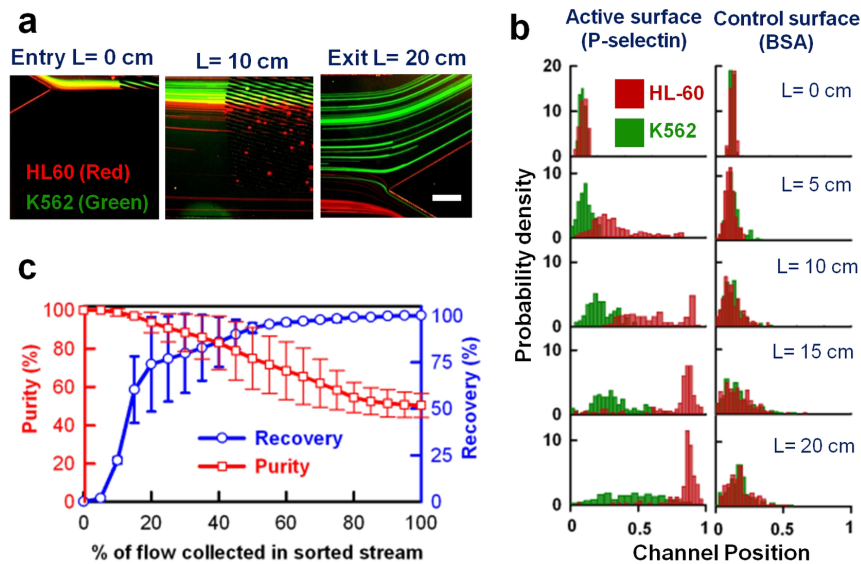


Figure 2 | Separation of HL60 and K562 cells using P-selectin patterns. (a) Overlaid fluorescence images (false colored) showing the distribution of the two cell types at different locations along the microchannel. Images were acquired via a continuous 10 s exposure for each fluorescence channel. Scale bar is 200 μm . (b) Evolution of distribution of the flux of the two cell types along the channel length shown as a dimensionless probability density normalized by the channel width. The result for the P-selectin patterns is shown against a control where BSA replaced P-selectin. (c) The purity (red) and recovery (blue) of HL60 cells at the channel exit ($L = 20$ cm) for different fractions of the total flow collected into the sorted stream as calculated from the observed probability density. For these experiments, a mixture of 5×10^5 cells/mL of each type in culture media was infused into the device parallel to a buffer stream at a wall shear stress of 0.5 dyn/cm^2 . Error bars indicate SD for $n = 3$ independent experiments.

indicating that the gold pattern did not significantly affect the cell distribution. The observed broadening of the cell distribution during separation on P-selectin may be attributed to weak interactions between the P-selectin and K562 cells.

Phenomenological model illustrates the mechanisms of cell separation. Quantitative understanding of the transport mechanisms of cell separation is essential for optimizing the device performance and guiding future development of AFF for other applications. We developed a phenomenological mathematical model that accounts for the major transport processes within the device which can be used for estimation of the separation performance (Fig. 3a).

The cells entering the device settle to the bottom of the channel under the action of gravity, with the settling length depending on geometry, flow velocity, and initial distribution of the cells. We observed that HL60 cells that settled to the bottom of the channel attached to the P-selectin stripes and tracked along their edges for a certain distance before detaching and reattaching on a downstream stripe (Supplementary Movie 1). The cells tracked along the edges of several consecutive P-selectin stripes, but then detached and traveled a long distance before re-attaching and tracking along the edges of another set of P-selectin stripes. These observations suggest that two different capture probabilities are at play during the repeated rolling and detachment of cells. The cells in the free stream flowing close to the surface can initiate rolling on the patterns with a relatively low probability, P_∞ ²⁰. These cells track the patterned edges for a certain distance (l_e) before detaching and reattaching to an immediately downstream stripe with a significantly higher probability, P_0 . For HL60 cells on P-selectin patterns, we determined the values of P_0 and l_e from experiments (See Supplementary Note), and combined the Davis & Giddings model for near wall particle setting under gravity²¹ with the Goldman's model for particle convection²² to describe the gravitational settling of the cells within the microchannel. Assuming that rolling along the edge is a Poisson process¹⁷ with the mean edge tracking length l_e depending on the angle of inclination (α) of the patterns, we performed a Monte Carlo

simulation to obtain the distribution of cells at different locations in the separation channel. The simulation results showed excellent agreement with the experimental results (Fig. 3b) for $P_\infty = 0.007$, which is only in modest deviation from the range of P_∞ determined experimentally (0.015–0.038). See Supplementary Note for a detailed description of the model and related experiments.

To obtain scaling relations between the fundamental separation parameters, we developed a simple analytical model that estimates the lateral displacement of the cells (see Supplementary Note). We found that the mean lateral displacement (D) scales linearly with length (L) as $D^* = L^*\theta$, where the scaling parameter θ is given by

$$\theta = \left(1 + \frac{b}{P_{eff} l_e \sin \alpha \cos \alpha} \right)^{-1} \quad (1)$$

Here, D^* and L^* are the normalized mean lateral displacement and length, respectively, given by $D^* = (D \cos \alpha)/b$ and $L^* = (L \sin \alpha)/b$, where b is the perpendicular distance between successive pattern edges (see Supplementary Fig. S5). The effective attachment probability (P_{eff}) combines the effects of P_0 and P_∞ and can be shown to be $P_{eff} = [1 + (1 - P_0)/P_\infty]^{-1}$ (see Supplementary Note). This scaling holds true when P_∞ is comparatively small i.e. when the length scale for separation dominates over the gravitational settling length; while the simulation results deviate modestly from the theoretical scaling predictions as the two length scales became comparable at larger values of P_∞ (Fig. 3c). The ratio of standard deviation (σ) of the lateral displacement to the mean displacement (D) is indicative of the separation resolution, which may be expected to depend on the number of stripes that the cells interact with (given by $L^* \cdot P_{eff}$ once the cells settle). It exhibits an initial peak in magnitude with increasing $L^* \cdot P_{eff}$ during the gravitational settling phase before transitioning to an inverse power law relation (Fig. 3d). The decreasing value of σ/D with increasing the number of stripes that the cells interact with is in accordance with theoretical scaling predictions (Supplementary Equation 8), and is analogous to the increased resolution observed in chromatographic separations for longer columns.

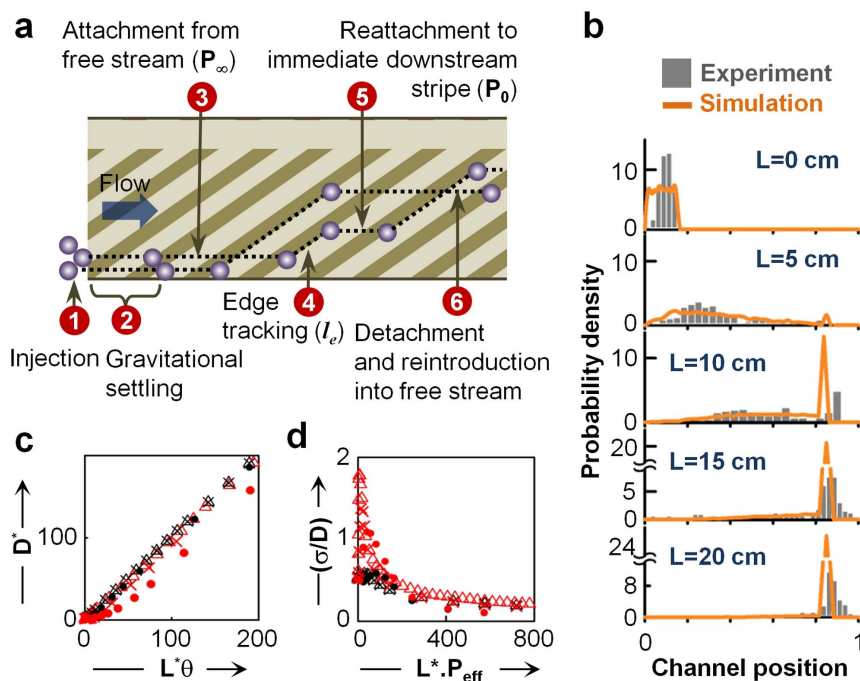


Figure 3 | Theoretical modeling of cell separation in the device. (a) Schematic description of the key processes governing the transport of cells inside the separation channel. (b) Comparison of the experimental distribution of the flux of HL60 cells for the same conditions described previously with that predicted by the model ($P_\infty = 0.007$, $P_0 = 0.95$, $l_e = 23.96 \mu\text{m}$). Channel position is normalized by the channel width. (c–d) Scaling relations between different operational parameters. Mean normalized lateral displacement (D^*) is proportional to the normalized length of travel (L^*) scaled by the non-dimensional parameter θ (c), while the ratio of standard deviation to mean lateral displacement (σ/D) scales with the number of patterns on which the cells roll (L^*P_{eff}) (d). Plots of simulated results are shown for different values of P_∞ (0.001 – \blacktriangle , 0.01 – \times , 0.9 – \bullet) and l_e ($10 \mu\text{m}$ – \blacktriangle , $100 \mu\text{m}$ – \blacktriangle).

Direct isolation of neutrophils from blood. The theoretical modeling of the cell separation process predicts that the edge tracking length (l_e) and attachment probability (P_∞) determine the channel length required for separation. Since P-selectin is known to differentially recruit neutrophils over other leukocytes *in vitro*²³, and the rolling behaviors of HL60 cells and neutrophils on P-selectin are similar (see Supplementary Fig. S6), we anticipated that HL60 cells were a good model for neutrophils and that the device could therefore be directly adapted for neutrophil isolation. To separate neutrophils, human blood anticoagulated with buffered sodium citrate²⁴ and diluted 1:1 with buffer was co-injected alongside a buffer stream that contained $30 \mu\text{M Ca}^{2+}$. This Ca^{2+} concentration was sufficient to enable P-selectin bond formation without causing blood coagulation. Within the separation channel, leukocytes rolled on the P-selectin patterns and were displaced from the blood stream into the parallel buffer stream, while the erythrocytes exhibited only a small lateral dispersion (Supplementary Movie 2; leukocytes can be fairly easily distinguished from erythrocytes by their morphology). By the end of the separation channel almost all of the erythrocytes remained on the blood input side and could be rejected, while a highly pure stream of leukocytes was obtained on the other side.

We collected 20% of the flow as the sorted stream and analyzed the device performance using flow cytometry to identify erythrocytes (GlycophorinA⁺ CD45⁻), leukocytes (CD45⁺ GlycophorinA⁻), neutrophils (CD66⁺ CD14^{low}), monocytes (CD14⁺ CD66⁻), lymphocytes (CD66⁻ CD14⁻) in the input, sorted, and waste streams (Fig. 4a,b). We found that the sorted stream consisted of highly pure population of leukocytes $99.6 \pm 0.3\%$ (up to 99.84%) representing a 0.4×10^6 fold enrichment over erythrocytes (Fig 4c). This enrichment ratio, calculated as the product of the ratio of target cells to non-target cells in the sorted stream and the ratio of non-target cells to target cells in the inlet stream (see Methods for the detailed expression), was three orders of magnitude higher than that typically

obtained in other chip-based continuous flow fractionation methods⁵. The sorted leukocyte population was highly enriched in neutrophils with purity $92.1 \pm 0.2\%$ (Fig 4d), representing a neutrophil enrichment ratio of 18,760 with respect to other cells, while the waste stream was significantly depleted of neutrophils. The neutrophil purity is comparable to existing methods of neutrophil separation by antibody capture⁴ and to the best of our knowledge is the first demonstration of using transient weak adhesive interactions to attain such high purities and enrichment ratios in a continuous flow system. Hematological staining revealed that 95% of the sorted neutrophils had segmented nuclei (41 out of 43 analyzed) typical of mature polymorphonuclear neutrophils (Fig. 4e). Staining with P-selectin further demonstrated that only leukocytes that exhibited high affinity for P-selectin were enriched in the sorted stream (Supplementary Fig. S7). In these experiments with 1:1 diluted blood the neutrophil recovery was estimated to be between 65–70% (see Supplementary Note). Although the device also worked with whole blood, the neutrophil recovery was 4-fold lower than with 1:1 diluted blood possibly due to increased steric hindrance by the erythrocytes or the presence of PSGL-1 in plasma²⁵.

Next, we investigated the effects of separation on the viability, activation state, and phagocytosis function of the neutrophils. Using the trypan blue dye exclusion assay we found the viability of the sorted cells to be $98.8 \pm 0.7\%$. Neutrophils are extremely sensitive to stimulus and can undergo rapid activation resulting in several phenotypic and morphological changes^{26–28}. To detect whether the sorted neutrophils were activated, we used the classical markers – L-selectin and Mac-1 – that are shed and up-regulated respectively upon activation²⁹. When compared to fresh whole blood and activated control, the sorted neutrophils exhibited minimal change in expression of L-selectin and Mac-1, indicating that they were not activated (Fig. 4g). The sorted neutrophils also successfully phagocytosed E.coli particles showing same level of phagocytotic activity as the neutrophils in whole blood

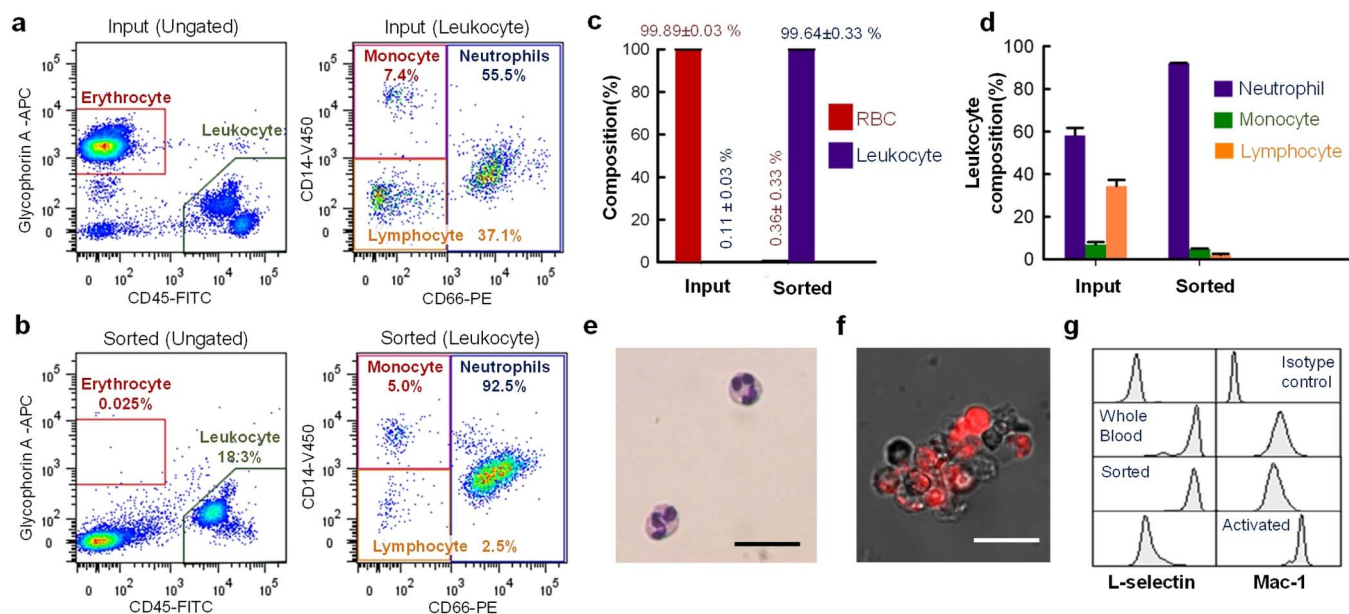


Figure 4 | Direct isolation of neutrophils from blood. (a,b) Phenotyping *via* flow cytometry analysis of the (a) input and (b) sorted samples. Input is depleted of erythrocytes to enable cytometry. (c,d) Graphical representation of the results from the flow cytometry analysis depicted as percent composition. (c) The ratios of erythrocytes and leukocytes in the samples before and after sorting demonstrate high erythrocyte rejection. (d) Composition of the leukocyte population in the sample before and after sorting demonstrate high degree of neutrophil enrichment. Error bars in (c) and (d) represent SD of $n = 3$ independent experiments. (e) Histological staining of the sorted sample showing polymorphonuclear neutrophils. (f) Overlaid bright-field and fluorescence images of the sorted neutrophils demonstrating successful phagocytosis of *E. coli* particles tagged with a pH-sensitive fluorescent dye. Scale bars are 20 μm . (g) Expression level of activation markers L-selectin and Mac-1 on neutrophils in sorted cells and fresh whole blood. Isotype control (negative control) and activated neutrophils (positive control) are shown for reference. For neutrophil separation, citrate anticoagulated whole blood was diluted 1 : 1 in the running buffer (supplemented with 30 μM Ca^{++}) and injected parallel to a stream of running buffer at a shear stress of 0.5 dyn/cm^2 .

when assayed using flow cytometry, indicating that the sorted cells were also functionally intact (Fig. 4f, Supplementary Fig. S8).

Label-free detection of neutrophil activation in blood. The ability to sort cells in continuous flow without extensive sample preparation is useful for point-of-care analysis as it greatly simplifies the device design, potentially enabling instrument-free disposable devices. Neonatal sepsis accounts for a large fraction of childhood deaths in developing countries, but diagnosis is challenging due to non-specific clinical symptoms¹⁵. While detection of neutrophil activation by up-regulation of CD64 has high diagnostic value³⁰, it requires flow cytometry that is typically not available in resource-limited settings. Given that activation of neutrophils reduces their efficiency of rolling on P-selectin³¹, we investigated whether the present method could be used to detect neutrophil activation in blood. A concept of such a device is shown in Fig. 5a, where a downstream detector counts the number of cells that are sorted out. Since background cells are rejected, the detector does not need to discriminate between the types of cells being sorted, analogous to a detector at the end of a chromatography column. If neutrophils are activated, we expect a decrease in the flux of sorted cells.

To test this concept, whole blood was activated *ex vivo* by incubation with either common physiological pro-inflammatory mediators (Lipopolysaccharide (LPS), Tumor Necrosis Factor- α (TNF- α) or Platelet Activation Factor (PAF)) or with buffer as control, and injected into the device following 1 : 1 dilution according to the same protocol used for neutrophil sorting (see Methods). In case of normal blood (incubated with buffer), neutrophils rolled on the edges and were separated from the blood stream as early as 10 min after injection. However, in the case of activated blood there was very little or no attachment of neutrophils to the P-selectin patterns and separation of cells from the blood stream did not occur (see Supplementary

Movie 3). We also did not observe sticking of neutrophils or platelets inside the device. We quantified the average flux of the sorted cells between 15 and 30 min after injection was started in a region 10 cm downstream of the inlet defined as shown in Fig. 5a (see Methods). Using blood samples from different donors, we found that the flux of sorted cells in activated blood was dramatically diminished as compared to a normal blood sample (Fig. 5b).

Discussion

We have demonstrated AFF using P-selectin as a model weak-affinity ligand. Apart from neutrophil separations, selectins have been shown to have potential to separate hematopoietic stem cells from bone marrow²⁵, $\text{CD}34^+\text{CD}38^+$ from $\text{CD}34^+\text{CD}38^-$ ³², and cancer cells from blood³³. Selectin-based separation of these cells has been limited to batch process requiring separate capture and release that yields relatively low purity^{25,33}. Devices with selectin-coated microstructures have also been employed for sorting^{34,35}, but have failed to sort cells from blood due to mixing of the flows leading to dispersion of the red blood cells, which does not occur in AFF due to the absence of lateral flows. Our results open new avenues for selectin-based sorting that overcome the limitations of batch processing in a format suitable for direct isolation in a flow-through device. The high-purity separation enabled by AFF is due to the absence of lateral fluid flows and the multiple molecular recognition events that gradually lead to lateral displacement, in contrast to approaches that utilize a single recognition event such as capture by high-affinity antibodies where non-specific adhesion directly impacts the purity³⁶.

Neutrophils were isolated within 30 min using AFF, which is significantly faster than the conventional density gradient isolation that requires ~ 1 h and involves multiple wash steps²⁸. While the purity of 92% with AFF is comparable to previous antibody based methods⁴ and density-gradient methods²⁸, the RBC rejection ratio (see

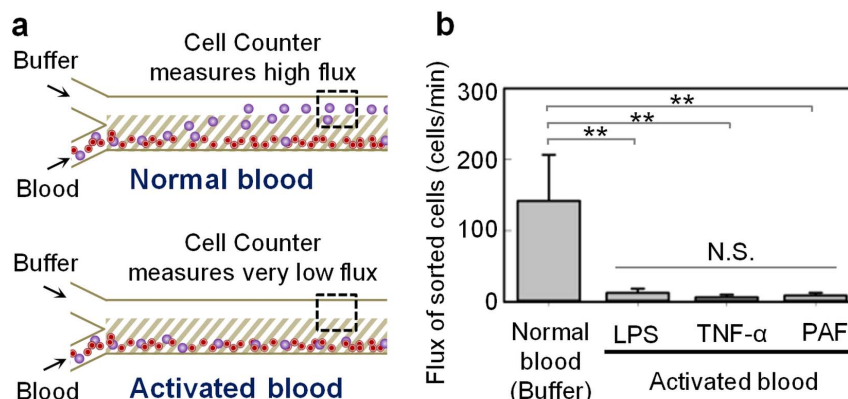


Figure 5 | Detecting neutrophil activation using activation-dependent cell sorting. (a) A cartoon showing the concept for detecting activation of neutrophils in blood. A narrow stream of blood is flowed parallel to a buffer stream on the asymmetric P-selectin patterned surface and an unbiased cell counter (that counts the flux of all cells separated from the blood stream) enumerates the sorted cells downstream of the inlet as shown. While neutrophils in normal blood separate from the blood stream at a high rate, activated neutrophils fail to separate due to lack of interaction with the P-selectin patterns leading to very low flux that correlates with the activated state of the blood. (b) Anticoagulated whole blood was activated *ex vivo* by incubation with LPS, TNF- α and PAF or buffer as control, and infused into the device after dilution (1 : 1) parallel to the buffer stream following the same protocol for separation. The flux of sorted cells was measured 10 cm downstream of the inlet averaged between 15–30 min post infusion. Blood activated using LPS, TNF- α and PAF as agonist resulted in significantly lower (** $p < 0.038$) flux of sorted cells when compared to time-matched samples of normal blood (incubated with buffer). Error bars show the SD of $n = 3$ independent experiments.

Methods) of AFF is highest reported amongst current continuous flow fractionation systems, for example - 400,000-fold with AFF compared to ~20-fold in microfluidic centrifugal sorting³⁷, 110-fold in micropost assay³⁸, ~2-fold (at optimum flow rate of 5 $\mu\text{L}/\text{min}$) in leukapheresis³⁹. We believe AFF may provide a method for rapid extraction of leukocytes and neutrophils from unprocessed blood to yield cells ready for biological assays or genetic analysis without requiring washing or other preparatory steps⁴⁰. The current device can process blood at ~1 $\mu\text{L}/\text{min}$ and is ideally suitable for analytical applications such as obtaining neutrophil counts and isolation of cells for genetic analysis. Given that most common blood cells exist at high concentrations (>10 to $10^4 \mu\text{L}^{-1}$) and standard automated counters typically analyze very small volumes (~10–50 μL)², similar results can be obtained in 20–30 min in our device. The system can potentially be massively parallelized to enhance the throughput which would enable processing large sample volumes extending to applications such as isolation and fractionation of stem cells for therapeutics.

Systemic activation of peripheral neutrophils is a fatal condition as it quickly leads to tissue damage and multi-organ failure²⁷, and is seen with end stage sepsis or severe systemic inflammation and is not common in most diseases. The present device can be potentially used to quickly detect activation in peripheral neutrophil population, prompting faster intervention and better prognosis. The low driving pressures (< 1 kPa) and small sample volumes ($<10 \mu\text{L}$ of blood and 200 μL of buffer) make the cell sorting method potentially compatible with use of capillary forces for device operation. While optical detection was used in the present work, we envision that cells may also be counted in a variety of ways ranging from collection of the sorted cells over a downstream filter for crude manual counting, to integrating simple capacitive sensors. Separation channels could potentially be arranged in series to sort cells based on more than one surface marker, or the sorted cells could be used for downstream analysis. AFF can potentially be extended to exploit other weak adhesive interactions for novel applications such as fractionation of sub-populations of lymphocytes or stem cells using E-selectin and VCAM^{41,42}, or to separate malaria-infected erythrocytes to aid malaria diagnosis⁴³. Antibodies⁴⁴, peptides, or other affinity molecules will need to be designed with optimum binding kinetics in order to enhance specificity and extend AFF as a generic cell isolation

technique. As such, the ability to sort cells with high purity in continuous flow stream offers new opportunities in analysis of cells, especially at the point-of-care.

Methods

Detailed methods are described in Supplementary Information. *Fabrication of receptor-patterned substrate and microfluidic device.* Gold coated slides (gold thickness 100 nm for HL60 experiments and 20 nm for blood experiments, 5 nm chromium adhesion layer) (EMF Corp, NY) were coated with OCG825 photoresist and patterned using photolithography (Supplementary Fig. S1) using Gold etchant and Chromium etchant (Sigma) followed by photoresist stripping in acetone. The patterned slides were then washed successively in acetone and ethanol, dried and stored for future use.

Surface functionalization of the patterned gold slides was performed using a modified version of a previously established method⁴⁵. The patterned slides were cleaned by immersing in piranha bath (3 : 1 H_2SO_4 to H_2O_2) maintained at 80°C for 10 min, washed with DI water and ethanol, and dried thoroughly. The slides were then immersed in a solution containing 1% (v/v) Polyethyleneglycol (10–12 units) trimethoxysilane (Gelest, PA) and 2% (v/v) Triethylamine (Sigma) in anhydrous Toluene (Sigma). The slides were incubated for more than 6 h at room temperature in a closed container after which they were removed, washed with acetone, and dried. Next, the slides were flooded with 5 mM solution of 3,3'-Dithiopropionic acid di(N-succinimidyl ester) (Sigma) in anhydrous Dimethylformamide (Sigma), placed on orbital shaker and incubated for 1 h. The functionalized slides were sonicated in an ethanol bath for 10 min, washed with ethanol, dried, and immediately used for protein immobilization.

The protein incubation was done in customized incubation chambers. Thin strips (~1 mm width) of Secureseal Adhesive sheet (250 μm thick) (Electron Microscopy Science, PA) were cut and pasted on the border of the functionalized slide. Next, inlet and outlet ports were drilled on a Hybrislip (Electron Microscopy Science, PA) before sticking on the adhesive strips previously placed on the slide. Human recombinant P-selectin (R&D Systems, MN) solution of desired concentration was made in Dulbecco's Phosphate Buffered Saline (DPBS) and was used to fill the chamber using a micropipette. The whole setup was placed in a humidified enclosure to prevent drying of the solution. For HL-60 separation experiments, 5 $\mu\text{g}/\text{mL}$ of P-selectin solution was incubated for 3 h while for blood separation experiments 15 $\mu\text{g}/\text{mL}$ of P-selectin was incubated for 1 h. The above protocol achieved a P-selectin site density of ~500 sites/ μm^2 for HL-60 separation substrates and ~1100 sites/ μm^2 for blood separation substrates measured as described below. After incubating for the desired time, the incubation chamber was removed from the slides using tweezers, and the slides were washed in a stream of DPBS for 1 min, placed in sterile 1% BSA solution (Teknova, CA), and stored at 4°C. The slides were used within 48 h of protein immobilization.

The microfluidic channel was cast in polydimethylsiloxane (PDMS) from a silicon master mold following standard soft lithography techniques. The PDMS channel was then aligned and reversibly attached with the patterned substrate *via* a vacuum manifold to assemble the device (Supplementary Fig. S1). The cell/blood sample was



periodically rocked to maintain homogeneity and prevent cell settling, and was injected into the device using pressure-driven flow (Supplementary Fig. S2).

HL60/K562 separation experiment. HL60 cells and K562 cells were stained using Cell Tracker Red and Cell Tracker Green (Invitrogen) respectively and mixed in 1 : 1 ratio to a final concentration of 10^6 cells/mL suspended in cell culture media. The mixture was injected into the device alongside a DPBS buffer stream (with Ca^{2+} and Mg^{2+}) flowing at 5.2 $\mu\text{L}/\text{min}$. The inlet pressure was adjusted such that the cell stream occupied 10% of the channel width (flow rate was ~ 0.4 $\mu\text{L}/\text{min}$). The total wall shear stress was 0.5 dyn/cm^2 , which was found to be optimal for separation efficiency (higher shear stresses decreased P_s). Samples were collected in polypropylene vials and analyzed within 3 h to determine purities. Sorting efficiency (r) was calculated using the formula:

$$r = \frac{P_s(P_w - P_i)}{P_i(P_w - P_s)} \times 100 \quad (2)$$

where P_i , P_s , P_w are the purities of the input, sorted and waste fractions, respectively.

Neutrophil separation from blood and sample analysis. All experiments involving human samples were approved by the Committee On Use of Humans as Experimental Subjects (COUHES) at MIT and the BWH Institutional Review Board. Blood was collected from consenting adult healthy donors who had not taken aspirin or other NSAIDs within 48 h prior to blood withdrawal in 1.5 mL citrate vacutainers (3.2% buffered sodium citrate) and was immediately used for experiments.

The running buffer was made by supplementing DPBS (-/-) with 30 μM CaCl_2 (Sigma) and 200 units/mL of Polymyxin B (Sigma). Unprocessed whole anticoagulated blood was diluted 1 : 1 in the running buffer and injected parallel to the buffer stream at a total wall shear stress of 0.5 dyn/cm^2 , which corresponds to a 5.2 $\mu\text{L}/\text{min}$ of buffer flow rate and 0.25 $\mu\text{L}/\text{min}$ blood flow rate, with a width of the input (blood) stream at $\sim 10\%$ of the channel width. The sorted neutrophils were either collected in HBSS (-/-) on ice (for the viability, activation, and phagocytosis assays) or in a 1% formaldehyde solution (for determining purity through flow cytometry). The enrichment ratio (E.R.) as defined in previously⁵, was calculated as follows:

$$E.R. = \frac{P_{t,\text{sorted}}/P_{nt,\text{sorted}}}{P_{t,\text{input}}/P_{nt,\text{input}}} = \frac{P_{t,\text{sorted}}(1 - P_{t,\text{input}})}{P_{t,\text{input}}(1 - P_{t,\text{sorted}})} \quad (3)$$

where $P_{t,\text{input}}$ and $P_{t,\text{sorted}}$ are purities of the target cells in input and sorted fractions respectively, and $P_{nt,\text{input}}$ and $P_{nt,\text{sorted}}$ are purities of the non-target cells in input and sorted fractions respectively (measured by flow cytometry). E.R. of leukocytes (which is same as rejection ratio of RBCs) is calculated considering leukocytes as target cells and RBC as non-target cells.

To detect activation, the device was modified to include four independent 10 cm-long channels on a single chip. Four 250 μL aliquots of blood were made soon after collection, and 25 μL of buffer (DPBS), LPS (10 $\mu\text{g}/\text{mL}$ in DPBS), TNF- α (10 $\mu\text{g}/\text{mL}$ in DPBS) and PAF (1 $\mu\text{g}/\text{mL}$ in DPBS) were added to each aliquot and incubated for 30 min at room temperature. The samples were diluted (1 : 1) in running buffer and injected in separate channels following the protocol described before. Time lapse images were acquired at the exit of each channel at regular intervals and were manually analyzed to obtain unbiased counts of cells separated from the blood stream. The experiment was performed in triplicate with independent samples.

- Cheng, X. *et al.* A microfluidic device for practical label-free CD4(+) T cell counting of HIV-infected subjects. *Lab Chip* **7**, 170–178 (2007).
- McPherson, R. A., Pincus, M. R. & Henry, J. B. *Henry's clinical diagnosis and management by laboratory methods*. 21st edn, (Saunders Elsevier, 2007).
- Bosio, A. *et al.* Isolation and enrichment of stem cells. *Adv Biochem Eng Biotechnol* **114**, 23–72 (2009).
- Kotz, K. T. *et al.* Clinical microfluidics for neutrophil genomics and proteomics. *Nat Med* **16**, 1042–U1142 (2010).
- Gossett, D. R. *et al.* Label-free cell separation and sorting in microfluidic systems. *Anal Bioanal Chem* **397**, 3249–3267 (2010).
- Hu, X. Y. *et al.* Marker-specific sorting of rare cells using dielectrophoresis. *Proc Natl Acad Sci U S A* **102**, 15757–15761 (2005).
- Karnik, R. *et al.* Nanomechanical Control of Cell Rolling in Two Dimensions through Surface Patterning of Receptors. *Nano Lett* **8**, 1153–1158 (2008).
- Edington, C. *et al.* Tailoring the trajectory of cell rolling with cytostatic surfaces. *Langmuir* **27**, 15345–15351 (2011).
- Nishimura, T., Miwa, J., Suzuki, Y. & Kasagi, N. Label-free continuous cell sorter with specifically adhesive oblique micro-grooves. *J. Micromech. Microeng.* **19** (2009).
- Alexeev, A., Verberg, R. & Balazs, A. C. Patterned surfaces segregate compliant microcapsules. *Langmuir* **23**, 983–987 (2007).
- Anderson, B. N. *et al.* Weak rolling adhesion enhances bacterial surface colonization. *J Bacteriol* **189**, 1794–1802 (2007).
- Tedder, T. F., Steeber, D. A., Chen, A. & Engel, P. The Selectins - Vascular Adhesion Molecules. *FASEB J* **9**, 866–873 (1995).
- Stone, J. D., Chervin, A. S. & Kranz, D. M. T-cell receptor binding affinities and kinetics: impact on T-cell activity and specificity. *Immunology* **126**, 165–176 (2009).
- Ley, K., Laudanna, C., Cybulsky, M. I. & Nourshargh, S. Getting to the site of inflammation: the leukocyte adhesion cascade updated. *Nature Reviews Immunology* **7**, 678–689 (2007).
- Chiesa, C., Panero, A., Osborn, J. F., Simonetti, A. F. & Pacifico, L. Diagnosis of neonatal sepsis: a clinical and laboratory challenge. *Clin Chem* **50**, 279–287 (2004).
- Al-Gwaiz, L. A. & Babay, H. H. The diagnostic value of absolute neutrophil count, band count and morphologic changes of neutrophils in predicting bacterial infections. *Med Princ Pract* **16**, 344–347 (2007).
- Lee, C. H., Bose, S., Van Vliet, K. J., Karp, J. M. & Karnik, R. Examining the Lateral Displacement of HL60 Cells Rolling on Asymmetric P-Selectin Patterns. *Langmuir* **27**, 240–249 (2011).
- Moore, K. L. *et al.* P-Selectin Glycoprotein Ligand-1 Mediates Rolling of Human Neutrophils on P-Selectin. *J Cell Biol* **128**, 661–671 (1995).
- Snapp, K. R., Wagers, A. J., Craig, R., Stoolman, L. M. & Kansas, G. S. P-selectin glycoprotein ligand-1 is essential for adhesion to P-selectin but not E-selectin in stably transfected hematopoietic cell lines. *Blood* **89**, 896–901 (1997).
- Zhang, Y. & Neelamegham, S. Estimating the efficiency of cell capture and arrest in flow chambers: Study of neutrophil binding via E-selectin and ICAM-1. *Biophys J* **83**, 1934–1952 (2002).
- Davis, J. M. & Giddings, J. C. Influence of Wall-Retarded Transport on Retention and Plate Height in Field-Flow Fractionation. *Sep Sci Technol* **20**, 699–724 (1985).
- Goldman, A. J., Cox, R. G. & Brenner, H. Slow Viscous Motion of a Sphere Parallel to a Plane Wall .2. Couette Flow. *Chem Eng Sci* **22**, 653–661 (1967).
- Reinhardt, P. H. & Kubes, P. Differential leukocyte recruitment from whole blood via endothelial adhesion molecules under shear conditions. *Blood* **92**, 4691–4699 (1998).
- Abbitt, K. B. & Nash, G. B. Characteristics of leucocyte adhesion directly observed in flowing whole blood in vitro. *Br J Haematol* **112**, 55–63 (2001).
- Narasipura, S. D. & King, M. R. P-selectin-coated microtube for the purification of CD45+ hematopoietic cells directly from human peripheral blood. *Blood Cells Mol Dis* **42**, 136–139 (2009).
- Borregaard, N. Neutrophils, from Marrow to Microbes. *Immunity* **33**, 657–670 (2010).
- Brown, K. A. *et al.* Neutrophils in development of multiple organ failure in sepsis. *Lancet* **368**, 157–169 (2006).
- Clark, R. A. & Nauseef, W. M. Isolation and functional analysis of neutrophils. *Curr Protoc Immunol* **Chapter 7**, Unit 7.23 (2001).
- Kishimoto, T. K., Jutila, M. A., Berg, E. L. & Butcher, E. C. Neutrophil Mac-1 and MEL-14 adhesion proteins inversely regulated by chemotactic factors. *Science* **245**, 1238–1241 (1989).
- Bhandari, V., Wang, C., Rinder, C. & Rinder, H. Hematologic profile of sepsis in neonates: neutrophil CD64 as a diagnostic marker. *Pediatrics* **121**, 129–134 (2008).
- Davenpeck, K. L., Brummet, M. E., Hudson, S. A., Mayer, R. J. & Bochner, B. S. Activation of human leukocytes reduces surface P-selectin glycoprotein ligand-1 (PSGL-1, CD162) and adhesion to P-selectin in vitro. *J Immunol* **165**, 2764–2772 (2000).
- Greenberg, A. W., Kerr, W. G. & Hammer, D. A. Relationship between selectin-mediated rolling of hematopoietic stem and progenitor cells and progression in hematopoietic development. *Blood* **95**, 478–486 (2000).
- Hughes, A. D. *et al.* Microtube device for selectin-mediated capture of viable circulating tumor cells from blood. *Clin Chem* **58**, 846–853 (2012).
- Chang, W. C., Lee, L. P. & Liepmann, D. Biomimetic technique for adhesion-based collection and separation of cells in a microfluidic channel. *Lab Chip* **5**, 64–73 (2005).
- Choi, S. Y., Karp, J. M. & Karnik, R. Cell sorting by deterministic cell rolling. *Lab Chip* **12**, 1427–1430 (2012).
- Mittal, S., Wong, I. Y., Yanik, A. A., Deen, W. M. & Toner, M. Discontinuous Nanoporous Membranes Reduce Non-Specific Fouling for Immunoaffinity Cell Capture. *Small* (2013).
- Wu, L. D., Guan, G. F., Hou, H. W., Bhagat, A. A. S. & Han, J. Separation of Leukocytes from Blood Using Spiral Channel with Trapezoid Cross-Section. *Anal Chem* **84**, 9324–9331 (2012).
- Davis, J. A. *et al.* Deterministic hydrodynamics: Taking blood apart. *Proc Natl Acad Sci U S A* **103**, 14779–14784 (2006).
- Sethu, P., Sin, A. & Toner, M. Microfluidic diffusive filter for apheresis (leukapheresis). *Lab Chip* **6**, 83–89 (2006).
- Abu al-Soud, W. & Radstrom, P. Purification and characterization of PCR-inhibitory components in blood cells. *J Clin Microbiol* **39**, 485–493 (2001).
- Tedder, T. F., Chen, A. J. & Engel, P. L-Selectin Regulation of Lymphocyte Homing and Leukocyte Rolling and Migration. *Cardiovascular Disease* **2**, 173–184 (1995).
- Thankamony, S. P. & Sackstein, R. Enforced hematopoietic cell E- and L-selectin ligand (HCELL) expression primes transendothelial migration of human mesenchymal stem cells. *Proc Natl Acad Sci U S A* **108**, 2258–2263 (2011).
- Ho, M. & White, N. J. Molecular mechanisms of cytoadherence in malaria. *Am J Physiol* **276**, C1231–1242 (1999).
- Miersch, S. & Sidhu, S. S. Synthetic antibodies: concepts, potential and practical considerations. *Methods* **57**, 486–498 (2012).



45. Veisoh, M., Zareie, M. H. & Zhang, M. Q. Highly selective protein patterning on gold-silicon substrates for biosensor applications. *Langmuir* **18**, 6671–6678 (2002).

Acknowledgments

The authors thank Prof. Ulrich H. von Andrian (Harvard Medical School), Prof. Krystyn Van Vliet (MIT), and Dr. Patricia L. Hibberd (Massachusetts General Hospital) for helpful discussions. Microfabrication was partly performed in the Microsystems Technology Laboratory (MIT). This work was supported by funding from the Deshpande Center for Technological Innovation at MIT (RK and JMK), NSF CAREER award 0952493 (RK) through the Chemical and Biological Separations program, and in part by NIH grants HL-095722 and HL-097172 (JMK), and the Cancer Center Support (core) Grant P30CCA14051 from the NCI.

Author contributions

S.B., M.H., C.S. and R.S. performed the HL60 separation experiments, S.B. performed the neutrophil separation experiments, S.B., R.S. and C.H.L. were involved in fabrication and characterization of the substrate. S.B. and R.K. developed the theoretical model and performed the simulations. D.D. contributed to design and analysis of experiments with blood. R.K. and J.M.K. directed the research project. S.B., R.K. and J.M.K. prepared the manuscript.

Additional information

Supplementary information accompanies this paper at <http://www.nature.com/scientificreports>

Competing financial interests: The authors declare no competing financial interests.

How to cite this article: Bose, S. *et al.* Affinity flow fractionation of cells via transient interactions with asymmetric molecular patterns. *Sci. Rep.* **3**, 2329; DOI:10.1038/srep02329 (2013).



This work is licensed under a Creative Commons Attribution-NonCommercial-ShareAlike 3.0 Unported license. To view a copy of this license, visit <http://creativecommons.org/licenses/by-nc-sa/3.0>